Simulating the Hydrodynamics of Self-Propelled Colloidal Clusters using Stokesian Dynamics

Yousef M. F. El Hasadi[1], Martin Crapper[2]

International Centre for Numerical Methods in Engineering (CIMNE), Edificio C1, Campus Norte, Jordi Girona 1-3,08034, Barcelona, Spain,

Email : Yme0001@Auburn.edu

Department of Mechanical and Construction Engineering Northumbria University, Ellison Place Newcastle -upon-Tyne, NE1 8ST

Abstract

Self-propelled clusters are involved in many technological applications such as in material science and biotechnology, and understanding their interaction with the fluid that surrounds them is of a great importance. We present results of swimming velocity and energy dissipation obtained through Stokesian dynamics simulations of self-propelled clusters. The clusters are of diffusion limited aggregates (DLA), consisting of force- and torque-free spherical particles. The number of particles per cluster ranges from 100 to 400, and with two fractal dimensions of 2.1 and 2.4. The clusters are self-propelled by imposing an explicit gait velocity applied in the x, y and z directions. It is found that the swimming velocity of the cluster and the energy dissipation are strongly dependent on the number of particles in the cluster and its fractal dimension, and on the orientation of the imposed explicit gait velocity. It was found that the rotational velocity of the self-propelled clusters decreases as the number of particles within the cluster is increased, n line with experimental observations reported recently in the literature.

Keywords: Clusters, Colloidal suspensions, Self-propelled, Stokesian Dynamics, active colloidal suspensions

1 Introduction

Colloidal particles are particles with a diameter ranging from 1 μm to 1 nm. They have a broad range of applications, such as in food [1], water treatment [2], energy storage [3], ceramics [4], living viruses [5], and blood cells [6]; further, a revolutionary technique for creating materials with specific properties based on the self-replicating colloidal clusters has emerged recently [7]. Colloidal particles form clusters when they are suspended in fluids, because the attractive forces acting on the particles overcome the repulsive ones [8]. In recent years, there have been significant advances in understanding the physics behind the fundamental structure of materials, and self-propelled particles have become a research priority due to their wide range of applications. Self-propelled particles can be defined as systems that are capable of independent self-propulsion by converting fuel into mechanical energy. Self-propelled particles can be divided into living and non-living particles. Examples of living particles are viruses, bacteria, and living cells. An example of non-living active matter is a gold –platinum bimetallic nano- rod in a solution of hydrogen peroxide, which propels by a reduction reaction, inducing a fluid flow along its surface through self-diffusiopheresis. The aggregation of self-propelled particles has gathered the attention of the scientific community, since understanding this will shed light on how groups of microorganisms swim [9, 10] and on building more sophisticated self-propelled micro-robots [11].

All the reported studies were concerned with untethered self-propelled clusters; however, there are numerous new applications for which tethered self-propelled clusters may be suitable, such as micro-machining systems powered by Janus particles (nanoparticles whose surfaces have two or more distinct physical properties) [12] and self-assembled colloidal asters [13] that exhibit locomotion and change in shape. Both of these applications have significant bearing on the development of microfluidic devices. However, to design and direct an assembly of particles with self-propulsion towards more complex structures such as clusters remains an unsolved problem both theoretically and experimentally.

Very recently, the self-assembly of active Janus particles has been reported. Zhang et al. [14] investigated the clustering of self-propelled Janus particles and bare silica particles in an electrical field. Both types of particles were of the order of microns in size, and the Janus particles are half metal-coated and interact with each other through electric-field-induced dipoles; the size of the particles was chosen such that they can be seen under an electron microscope. The particles were

suspended in water, and the electrical field induces a single dipole in the centre of the silica particles, while for the Janus particles, the same electric field induces one dipole in the half-coated hemisphere and another dipole in the silica hemisphere, with both dipoles being shifted from the centre of the sphere, which helps to induce anisotropic interactions. The propulsion of the Janus particles is controlled by the applied voltage. The electrically-induced dipoles are repulsive when their connection is perpendicular to the direction of the electrical field, and attractive if they are aligned with it. For the case of Janus particles with a size of 3 μm and silica particles 4 μm in diameter, Zhang et al. [14] observed the formation of chiral clusters, with the attraction between the silica and Janus particles overcoming the repulsion between the Janus particles themselves. All the elements of the clusters formed rotated either clockwise or anticlockwise. The rotating clusters took the shape of either tetrahedral (assembled at a high activity of particles) or square pyramids (constructed at a low activity); for both cases the silica particle is the hub. Interestingly, the clusters did not only rotate but also translated, due the collisions of the loose Janus particles, but also due to the imperfect rotational symmetry. The translation of those clusters has some similarity with the motion of some natural chiral micro-swimmers whose movement is driven by spiral-shaped flagella. The parameters that affected the shape of the cluster formation were the activity of the Janus particles, the hydrodynamic interactions and the dipole interactions between the particles. Also, if the ratio between the size of the hub silica particles and the Janus particles increased, the clusters formed different shapes. It was also observed that as the number of the particles increased, the clusters stopped rotating.

In the same research group, Yan et al. [15] proposed strategies to reconfigure active colloidal particles to collective states by imposing imbalanced interactions between the particles. They used molecular dynamics simulations and experiments as a proof of concept of their ideas. They obtained different forms of collective states, such as chains, clusters, isotropic gas swarms, vortices, jammed regions and polar waves, just by changing the intensity of the electrical field.

As shown in [14 and 15] self-propelled colloidal clusters are a feasible concept that may open the door to a wide range of applications from multi-tasking nano- robots to smart materials, and finally mimic biological life. However, understanding the phenomena of self–propelled clustering requires an understanding of the interaction of those clusters with their surrounding fluid. For non-active colloidal suspensions (i.e. non-self-propelled particles), there is a large body of literature

that investigates their behaviour theoretically and experimentally. There are three main numerical methods that been used to simulate colloidal suspensions with different resolutions of the hydrodynamic interactions, these being Stokesian dynamics [16], the lattice-Boltzmann method [1] and the boundary elements method [18].

Keaveny and Maxey [19] numerically investigated the swimming of an artificial micro-swimmer consisting of an artifical filament attached to a human blood cell. They assumed that the body of the swimmer consisted of equal-sized spherical particles arranged in a straight chain, and they used the force-coupling method (based on Stokesian dynamics theory) to calculate the configuration-dependent resistance tensor, in order to determine the hydrodynamic forces. Ishikawa et al. [20] analytically calculated the far- and near-field hydrodynamic interactions between two micro-organisms. The intermediate hydrodynamic interactions were calculated numerically by using the boundary element method. The micro-organisms were modelled as squirming spheres. They obtained numerical results for the transitional and rotational velocities, and the stresslet. Swan et al. [21] developed a theoretical and numerical framework which combines Stokesian dynamics and rigid body mechanics for the simulation of the swimming process of bodies at low Reynolds numbers. They assumed that the swimmer was composed of equal-sized spherical particles, which all move in a constrained way bounded by rigid body mechanics. They assumed that there were no external forces or fields acting on the particles. They investigated two types of swimmers, implicit gait swimmers where the surface velocity is not specified, and explicit gait swimmers were the velocity of the surface is specified. They reported energy dissipation curves for these different types of swimmers.

To better design autonomous micro-vehicles, and to understand how micro-organisms swim, an understanding of hydrodynamic properties of self-propelled clusters such as swimming velocity and energy that dissipates to the surrounding fluid are essential. To the best knowledge of the authors, ours is the first attempt to report data for the swimming velocity and energy dissipation rate of diffusion limited aggregate (DLA) clusters with different numbers of particles, fractal dimension, and orientation of the explicit gait velocity that propels the cluster. Our clusters are created from spherical particles that are constrained to swim as one rigid body. The main numerical method we use is the Stokesian dynamics method, which determines the velocity and trajectories of the individual particles. Then, those velocities and trajectories are used to determine the

swimming velocity and trajectory of the clusters, after incorporating the special laws developed for the swimming of bodies under a Stokes flow regime.

2 Mathematical Model and Numerical Technique

2.1 Stokesian dynamics

Particles at the colloidal size experience a wide spectrum of forces compared with those at the molecular size. The particles at colloidal size interact with each other based on continuum inter-particle effects such as the attractive Van der Waals and the repulsive screened electrostatic forces. However, the most elusive of them is the hydrodynamic force that results from the interaction of the particles with the surrounding continuum fluid. The hydrodynamic force can manifest into a long range component responsible for multi-body interactions, and a short range lubrication force, which is pair-wise in nature and plays a significant role in the rheology of highly concentrated colloidal suspensions.

Stokesian dynamics is a numerical simulation method that been developed specifically for the prediction of colloidal suspension microstructure. Introduced to the scientific community in the mid-80s by Brady and Bossis [16], it was the first simulation method that included both the long range and short range hydrodynamic interactions. The simulation method is based on molecular dynamics ideas, where the colloidal particles are treated as discrete entities, while the fluid that surrounds them is approximated to a continuum. The main difference between Stokesian dynamics and other methods available is that the former includes the exact form of the hydrodynamic interactions through the inclusion of the analytical solution of the hydrodynamic interaction of two spheres [22]. The hydrodynamic interactions are incorporated in the resistance and mobility tensors, and those tensors are dependent on the configuration of the particles, as will be shown later in this section.

Everything starts with applying Newton's equations of motion for a single particle. For the current case that particles are colloidal in size and the particle Reynolds number is very low (Re < 1), the inertia of the particles can be neglected. The forces and torques on the particles are then given from:

$$0 = F + F^{p} \tag{1}$$

where F^p is any force and torque of a non-hydrodynamic nature acting on the particle, such Van der Waals or electrostatic forces; in the current investigation we neglected theses forces for simplification reasons. At the length scales under consideration here, another force may be active, which is the Brownian force as a result of the bombardment of the particles by fluid molecules. However, this force can be neglected, since we assume that the particles are acting within a cluster. The hydrodynamic forces on the particles are given by:

$$F = -R_{FU}.U - R_{FE}:E \tag{2}$$

U and *F* are vectors of size 6N, where N is the number of particles. *U* is the velocity vector that contains the translational and rotational velocities of the particles, while *F* is the force vector that contains the forces and torques acting on the particles, and *E* represents the first moment of the surface velocities at the particle surface. It is a symmetric traceless tensor with a size of 5N. it is important only when implicit gait is utilized. R_{FE} represents the configuration-dependent resistance tensor that couples forces and torques with the first moments E. R_{FU} represents the configuration-dependent resistance tensors that couple the forces with velocities, and is called the grand resistance tensor. It has a size of 6Nx6N. R_{FU} consists of three second rank tensors, and it couples the forces, and torques on the particles to their transitional and angular velocities:

$$\begin{pmatrix} A & \tilde{B} \\ B & C \end{pmatrix} \tag{3}$$

where $\tilde{B}$ is the transpose of B. The second order tensors are given from the following relations for the case of two particles α and β as in [22]:

$$A_{ij}^{\alpha\beta} = X_{\alpha\beta}^{A} r_i r_j + Y_{\alpha\beta}^{A}(\delta_{ij} - r_i r_j) \tag{3a}$$

$$B_{ij}^{\alpha\beta} = Y_{\alpha\beta}^{B} \epsilon_{ijk} r_k \tag{3b}$$

$$C_{ij}^{\alpha\beta} = X_{\alpha\beta}^{C} r_i r_j + Y_{\alpha\beta}^{C}(\delta_{ij} - r_i r_j) \tag{3c}$$

The functions $X^A_{\alpha\beta}, Y^B_{\alpha\beta}$ and $X^C_{\alpha\beta}$ are scalar functions that depend on the separation distance between the particles. r, δ_{ij}, and ϵ_{ijk} are the unit vectors of particle position, Kronecker delta, and the permutation symbol respectively. The grand resistance tensor has two mathematical properties, that it is symmetric, and that it is positive definite. The last property is necessary to ensure that the particles will dissipate energy when they are suspended in the fluid.

The Stokesian dynamics method starts with expansion of the integral equation of the velocity of the particle, following [23]:

$$u_i(x) = u_i^{\infty}(x) - \frac{1}{8\pi\mu}\sum_{\alpha=1}^{N}\int_{Sa} J_{ij}(x-y) f_j(y) dS \tag{4}$$

$u_i^{\infty}(x)$ is the velocity field without particles, S_α is the surface of particle α, y is the location on the particle surface and x represents the location of the rigid particle centre in the continuum fluid field. J_{ij} is the space Green function also known as the Stokeslet or the Oseen tensor. It is expressed as the following:

$$J_{ij} = \frac{\delta_{ij}}{r} + \frac{r_i r_j}{r^3} \tag{5}$$

$f_j(y)$ is the force density at the point location y at the surface of the particle. The integration indicates that the summation must be conducted around all the particle surfaces. The total force on particle α, $F_{\alpha,}$ and the torque T_α are given from the following relations:

$$F_j^a = -\int_{Sa} f_i(y)\, dS_y \tag{6a}$$

$$T_i^a = -\int_{Sa} \varepsilon_{ijk}(y_i - x_j^a) f_k(y) dS_y \tag{6b}$$

The following step is to expand Equation 4 in moments about the x^α of each particle as follows:

$$u_i(x) - u_i^{\infty}(x) = -\frac{1}{8\pi\mu}\sum_{\alpha=1}^{N}\int_{Sa} J_{ij}(x-x^a) f(y)_j dS_y + \int_{Sa}\frac{\partial}{\partial y_k} J_{ij}\Big|_{\;y=x^a}(y_k - x_k^a) f_j(y) dS_y \tag{7}$$

Equation 7 represents the velocity of the particle at any point in the fluid, as a multipole moment. The disturbance that a single sphere in unbounded fluid creates is given by the following:

$$u_i' = \frac{1}{(8\pi\mu)}\left(1 + \frac{1}{6}a^2\nabla^2\right) J_{ij}(x-x^a) F_j^{\alpha} \tag{8}$$

Finally, the velocity at any point in the fluid can be conveyed in terms of the forces and torques applied by the particles on the fluid, as the in the following expression:

$$u_i(x) = u_i^{\infty} + \frac{1}{8\pi\mu}\sum_{\alpha}\left(1 + \frac{1}{6}a^2\nabla^2\right)J_{ij}F_j^a + \varepsilon_{ijk}\frac{r_k}{|r|^3}T_j^a \quad (9)$$

To compute the velocity of the individual particles from Equation 9, Faxen expressions for a single sphere are employed, and the translation and angular velocities of the single particle are:

$$U_i^a - u_i^{\infty}(x^a) = \frac{F_i^a}{6\pi\mu a}\left(1 + \frac{1}{6}a^2\nabla^2\right)u_i'(x_a^{\infty}) \quad (10a)$$

$$\Omega_i^a - \Omega_{\mathrm{i}}^{\infty} = \frac{T_i^a}{8\pi\mu a^3} + \frac{1}{2}\varepsilon_{ijk}\nabla_j u_k'(x^a) \quad (10b)$$

Writing Equation 10 for each particle, the grand mobility matrix M^{∞} is constructed. This relates the translational/angular velocity of the particles to their forces/torques. The grand mobility tensor can be related to that of the grand resistance tensor by:

$$M^{\infty} = R^{-1} \quad (10b)$$

The calculation of the values of the grand mobility tensor is done in a similar way to that of the resistance tensor. For more details about the derivation, readers can refer to the Appendix that accompanies [23]. The main output of the Stokesian dynamics algorithm is the velocity of the particles; then their positions can be calculated. The velocity of the particles is given as a function of the grand resistance matrix and the applied forces by:

$$U = R_{FU}^{-1}.(F^p R_{FE} : E) \quad (11)$$

After this very brief overview of the mathematical nature of the Stoksian dynamics method, we summarize, the necessary steps needed to implement the method computationally. The Stokesian dynamics method consists of the following main steps:

- Calculate the grand mobility tensor $M^{\infty} = R^{-1}$, where R the grand resistance tensor. The mobility tensor represents the many-body far field hydrodynamic interactions.

- The analytical, pair-wise resistance tensors are calculated for particles that are closer than a certain distance. This is denoted as $R^{2B,exact}$ and includes the effects of hydrodynamic lubrication.
- The truncated grand mobility tensor is calculated for each near particle pair subject to the same cut -off distance as in the previous step. This is referred as $R^{2B,\infty}$, since it represents the far field and pair-wise lubrication interaction between nearly touching particles.
- The grand resistance tensor is calculated as the following:

$$R = (M^{\infty})^{-1} + R^{2B,exact} - R^{2B} \quad (12)$$

The many-body far-field hydrodynamic interactions are included by the inversion of the grand mobility tensor, and the near-field lubrication interaction through adding $R^{2B,exact}$.

In the preceding explanations, particles have been treated as individual entities. However, we are now assuming a cluster acting as a rigid body with spherical particles as its constituents. The brief overview of the numerical implementation of the Stokesian dynamics method above applied to free particles suspended in a liquid; in the coming sections we will illustrate how we can link the Stokesian dynamics method with the mechanics of rigid bodies to calculate the hydrodynamic proprieties of swimming clusters constructed from spherical particles.

2.2 General hydrodynamic principles of self-propelled micro-bodies

It is essential to summarize very basic principles of the hydrodynamics of self-propelled bodies under a Stokes flow regime. A swimming self- propelled body swims through a fluid in such way that the velocity of the fluid at the surface of the swimmer is given by [21]:

$$u = \sum^{T} \bar{U} + u_s(t) \quad (13)$$

Where:

$$\sum = \begin{pmatrix} 1 & 0 & 0 \\ 0 & 1 & 0 \\ 0 & 0 & 1 \\ 0 & r3 & -r2 \\ -r3 & 0 & r1 \\ r2 & -r1 & 0 \end{pmatrix} \tag{14}$$

r represents the distance from the swimming body centre to a point on its surface, $\bar{U}$ is the six dimensional vector that contains the transitional and rotational velocities of the swimmer. $u_s(t)$ represents the deformation of the self-propelled surface which is necessary for swimming in low Reynolds number flows [21], known also in the literature as swimming gait. The prescribed time-varying deformation of the surface of the swimmer is given by the velocity of the swimmer surface, which is known as the swimming gait, $u_s(t)$. Mathematically, there are two ways to define swimming gait; one is to obtain it by calculating the first moments of velocity at the particle surfaces, E, referred to as *implicit* swimming gait, because the surface velocity mechanism is not specified. The alternative method, for larger deformations of the swimmer body, is to define an *explicit* gait velocity by directly adding an additional component to the velocity of the particles relative to the rigid body velocity. In our current investigation we choose an explicit gait velocity scheme in which two neighboring particles are assigned equal and opposite velocities, the magnitude of which do not change with time. This leaves the system locally force-free.

It should be noted that our swimmers are different from squirmers, since they do not utilize quadrupolar movements to move. However, they are much more related to phoretic active particles, which move by the deformation of their surface.

The swimming velocity of the self-propelled body is then determined from the following relation:

$$\bar{U} = -\left(\int_{S(t)} \sum{}^{T}\right)^{-1} \left(\int_{S(t)} \sum R \; u_s(t) dS\right) \tag{15}$$

In the current and previous sections, we have explained the principles of the two main parts of the numerical method that we use to determine the hydrodynamic properties of swimming clusters. In the coming section, the mechanics of the rigid body will be introduced, which are essential for keeping the particles that construct the cluster as a single body. Also, the equations governing the

swimming of the self-propelled clusters, deriving from the Stokesian dynamics method and the hydrodynamics of self-propelled bodies, will be introduced.

2.3 Mechanics of rigid assemblies

The preceding section discusses the simulation method for the dynamics of individual particles; however, we wish to represent a swimming cluster as an assembly of spherical particles. Thus, we need to impose some constraints such that if there is no gait (i.e. no deformation), the cluster will behave as a rigid body. Due to the linearity of the Stokes flow considered, the deformation and the rigid body response can be considered individually.

Here we introduce the essential rigid assembly laws that keep the cluster as rigid body. The velocity of cluster is given from the following equation:

$$\bar{U} = -\left(\sum R_{FU} . \sum^{T} \right) . \sum . (R_{FE} : E) \tag{16}$$

Where $\sum^{T}$ is the operator that projects the kinematics of the rigid assembly onto the velocity of the particles that constitute the cluster $\left(U = \sum^{T} . \bar{U}\right)$. $(\sum . R_{FU} . \sum^{T})$ is the resistance tensor governing the hydrodynamic interactions of the rigid assembly, not of the individual particles.

For the self-propelled clusters of the explicit gait type, a specified velocity is imposed on each particle in the cluster, and the velocity of the whole assembly of the particles will be given as the following:

$$U = \sum^{T} \bar{U} + u_s(t) \tag{17a}$$

$$\bar{U} = -(\sum . R_{Fu} . \sum^{T}) . \sum R_{FU} . u_s(t) \tag{17b}$$

$u_s(t)$ is the explicit swimming gait and specifies the kinematics of the swimming body relative to its rigid body motion. In order for any object to swim at low Reynolds number, it needs to deform its surface. The explicit gait velocity represents the velocity resulting from this deformation. If the gait velocity is zero, the collection of particles will move as a rigid body (i.e. a non-self propelling cluster).

The rate of energy dissipated by the fluid, or the work done by the swimmer, is given by the following equation:

$$\dot{E} = -F^C . U_s(t) \tag{18}$$

Where F^C is given as the following:

$$F^C = -F^p + R_{FU} . U \tag{19}$$

The computer code provided by Swan et al. [21] has been used after modification to suit our investigation. The code was validated by computing the drag coefficient in the x and y directions (CF1 and CF2 respectively) for a straight chain of particles. The results are compared with the numerical results of Durlofsky et al. [23] and with the analytical results of Chwang and Wu [24]. The drag coefficients in the horizontal and vertical directions are plotted against the number of particles in the chain, as shown in Figure 1. The comparison between our results and those of the literature is satisfactory.

3 Results

For our investigation, we have selected two different groups of DLA clusters with two different fractal dimensions (Kf = 2.1 and 2.4); the clusters were created from spherical particles of equal size, and the particles are force and torque free. The number of the particles was varied between 100 and 400. The clusters for simulation were generated using the DLA/TEM software [25]. This algorithm uses a constant fractal dimension for each aggregation step. During the DLA phase, the primary particles are produced at long distances from the centre of the mass of the aggregate. Then, to simulate the random motion of the primary particles, their trajectories aare decomposed into small step increments. We controlled the separation distance between the particles through the DLA/TEM software function, so the particles do not touch. A sample of the aggregates used is shown in Figure 2. The clusters are propelled by imposing an equal and opposite velocity ($U_s(t)$) to each neighboring pair particles, as shown in Figure 3. The energy dissipation and the swimming velocity of the cluster are then calculated for different configurations, ensemble averaging results over several realizations.

The variation of the non-dimensional transitional swimming velocity U/U_s of the cluster, together with the number of particles in the cluster, for the three different cases in which U_s is applied in the x, y, and z directions respectively for Kf = 2.1 are shown in Figure 4 (the initial configuration and orientation of the clusters is the same for all gait velocity orientations). The swimming velocity

variation with the number of particles is nonlinear. The figure shows that there is an optimum number of particles in which the cluster will have maximum velocity. This is an interesting observation that will help to better design self-propelled clusters. The general observation is that the swimming velocity of the cluster decreases as the number of the particles is increased. The translational swimming velocity of the cluster is sensitive to the direction of the application of the explicit swimming gait; it is clear that when the explicit gait velocity is applied in the x direction it always produces a higher swimming velocity until N = 300. The explanation of this behaviour may be due to the sensitivity of the swimming velocity to the geometry of the cluster, and not only to the number of particles. To investigate the effect of the geometry and the configuration of the particles on the swimming velocity of the cluster, the fractal dimension of the cluster was increased to 2.4. The variation of the swimming velocity with the number of particles for the case of Kf = 2.4 averaged over several realizations is shown in Figure 5. The clear difference between the behaviour of the clusters with Kf = 2.1 and 2.4 is that for the latter case, the local minima are more distinct than the local maxima, which is an opposite behaviour from that of clusters with Kf= 2.1. This shows that the geometry of clusters plays an essential role in determining the swimming velocity of the cluster.

A direct comparison between the swimming velocity for the cluster geometries with Kf = 2.1 and 2.4 for the case of U_s applied in the x direction is shown in Figure 6. The swimming velocity for the cluster with Kf = 2.1 is higher than that with Kf =2.4 as shown in Table 1. The swimming velocity for the cluster with Kf = 2.1 is 5.5 times higher than that of cluster with Kf = 2.4 when N = 250. For the case of Kf = 2.1, and especially when N = 250, the cluster consists of several branches, which may help in the swimming process by enhancing hydrodynamic interactions. Meanwhile, for case of Kf = 2.4, the cluster took a more spherical shape, as shown in Figure 7.

It is known that objects subjected to a Stokes flow regime can translate and rotate at the same time. This coupling between the two motions is reflected in the resistance and mobility functions. After we examined the variation of the transitional velocity of the cluster with the number of particles and the direction of the gait velocity, we attempted to illustrate the variation of the swimming angular velocity with the same parameters.

The variation of the angular swimming velocity is shown in Figure 8 and Kf =2.1. It has a wavy behavior like its translational counterparts, with the local maximum for the case considered at

around N = 150. However, as the number of particles increases, the swimming angular velocity decays rapidly. Similar observations have been reported by [14] were the clusters stopped rotating as the particle number increased. Further, if we increase the fractal dimension to a value of 2.4, at N = 150, all the cluster configurations show a local minimum, especially for the clusters with an explicit gait velocity applied in the z-direction. This is a reversed observation from the previous case. A similar dissipation of angular swimming velocity was noted at Kf=2.4.

The only interaction mechanism we have considered is that of hydrodynamic interaction. It is well known that hydrodynamic interactions are strongly dependent on the configuration of the particles, and also they are long and short ranged. In the current investigation, the far field and short range lubrication interactions are included in the simulation. Further investigation is required in order to understand which geometry is more energy efficient.

Another important parameter for the proper design of self-propelled clusters is the rate of energy dissipation during the swimming process.

The variation of the non-dimensional energy rate ($E' = \frac{\dot{E}}{6\pi\mu a U_S^2}$) with the number of particles for the three different cases were the explicit gait is oriented along the three main principal axes (x, y and z) and for the cluster geometry of Kf = 2.1 is shown in Figure 10. The variation is nonlinear, and takes a wavy trend. For a number of particles less than 200, the case in which the explicit gait velocity is applied in the x direction gives the lowest energy dissipation rate, while as the number of particles in the cluster increases, the case with the explicit gait applied in the y direction produces the lowest energy dissipation rate. The figure shows that the energy dissipation rate is a strong function of the number of the particles and the orientation of the explicit gait velocity. The increase of the energy dissipation with number of particles can be explained by the increase of the disturbance in the flow. Figure 10 shows that arrangement of the particles within the cluster also plays an essential role, since the local maximum and minimum of the swimming velocity for the three different orientations of the explicit gait velocity do not coincide with each other. This shows that, even when increasing the number of particles, an optimized energy dissipation rate can still be achieved. Equation 19 shows that the connecting force (F_c) is only a function of the resistance tensor that relates the velocity with force (i.e. R_{FU}), since neither the effect of the inter-particle

forces nor the shear rate was considered. R_{FU} is strongly dependent on the configuration of the particles in the cluster, which explains the fluctuation in the energy dissipation in Figure 10.

To investigate further the effect of the geometry, the fractal dimension of the clusters was increased to 2.4, and its effect on the energy dissipation is shown in Figure 11. For a number of particles less than 250, the variation of the rate of energy dissipation with the number of particles is nearly linear, with the explicit gait velocity orientated in the x direction generating more dissipation of energy than that in the y and z directions. However, as the number of particles increases, the variation starts to be non-linear, with the local minimum located for three cases at N = 300. Beyond this, the energy dissipation increases with the number of particles. A comparison between clusters of different fractal dimensions is shown in Figure 12. The energy dissipation for the clusters with Kf = 2.4 is lower than that of clusters with Kf = 2.1 for lower numbers of particles. However, as the number of the particles in the cluster increases, the energy dissipation becomes comparable for the two fractal dimensions considered.

In order to further investigate the effect of the fractal dimension on transitional velocity and the energy dissipation, the limited case of the gait velocity directed in the x-direction was chosen, and several values of the fractal dimension were selected. Due to the limitations of the software used for the generation of the clusters, we could not extend the range of the fractal dimensions used beyond that shown in Figure 13. For the values of the fractal dimension selected, the cluster with Kf = 2.1 exhibits the highest translational velocity for the greatest range of the particles used. This may be explained by considering that for Kf = 2.1 the shape of the clusters is between a rod and a sphere. Another noticeable observation from Figure 13 is that at higher values of Kf such as 2.5 and 2.6, the absolute translational velocity decreases significantly. Also, the fluctuations in the variation of the velocity with the number of the particles is deceased substantially at higher Kf values; this could be because the particles within the cluster are arranged in a nearly spherical shape.

The cluster with Kf = 2.6 dissipates the lowest amount of energy compared with other clusters, as shown in Figure 14. This indicates that considering the energy principle, self-propelled clusters with approximately the same value of Kf are most likely to form from a self-assembly procedure similar to that described in [14], which could explain why the clusters formed experimentally in [14] took a spherical shape.

4 Conclusions

A Stokesian dynamics simulation was conducted for diffusion limited aggregation (DLA) self-propelled clusters. The clusters consisted of force- and torque-free spherical particles, and were generated for different fractal dimensions Kf = 2.1 and 2.4. The clusters were self-propelled by imposing a velocity on the particles (explicit gait velocity). The following conclusions are drawn:

- The swimming velocity of the cluster is dependent on the number of particles, the fractal dimension, and the orientation of the explicit gait velocity.
- The variation of the swimming velocity with the number of the particles and the explicit gait velocity is nonlinear.
- The clusters with fractal dimension Kf = 2.1 exhibit higher swimming velocity than for the case of Kf = 2.4.
- The variation of energy dissipation with number of particles and the explicit gait velocity is non-linear.
- The effect of the fractal dimension on energy dissipation is more pronounced at lower numbers of particles in the cluster. However, as the number of the particles increases, the effect of fractal dimension becomes negligible.
- The translational velocity is decreased as the value of Kf is increased.
- The energy dissipation decreases with Kf, especially at higher values of Kf.

For the future, a more detailed analysis should be conducted relating the geometrical parameters with the Eigenvalues of the resistance tensors, in order to shed more light on our results. However, the current results may help to better design nanoparticles that specifically target cancer cells as in [26].

5 Acknowledgments

This research was conducted under the EU Framework 7 Marie Curie ITN Grant Number 607453: T-MAPPP: Training in Multiscale, MultiPhase Particulate Processes, for which we express our gratitude. Also, we wish to thank all members of EDEM (previously known as DEM solutions), and especially Stephen Cole for support for conducting the research.

6 References

1. Sanguansri, P., and Augustin, M., 2012, "Nanoscale materials a food industry perspective", Trends in Food Science and Technology, Vol.17 (10), pp. 5547-556.
2. Edzwald, J. K., 1993, "Coagulation in drinking water treatment: Particles, organics and coagulants", Water Science Technology, Vol. 27, pp. 21-35.
3. El Hasadi , Y. M. F., and J. M. Khodadadi, 2013, " Numerical simulation of the effect of the size of the suspensions on the solidification process of nanoparticle- enhanced phase change materials", Journal of Heat Transfer, Vol. 135, p.052901.
4. Deville, S., Maire, E., Bernard-Granger, G., Lasalle, A., Bogner, A., Gauthier,C., Leloup, J., and Guizard, C., 2009, "Metastable and Unstable Cellular Solidification of Colloidal Suspensions," Nature Mater., Vol.8, pp. 966–972.
5. Blach, M. W., Vaughn, J., Novotny, J., Drapeau, T. D., Vailancourt, R., Lapierre, J., and Ashe, A., 2000, "Light scattering by viral suspensions ", Limnol Oceanogy, Vol. 45, pp. 492-498.
6. Price, R. J., Skyba, D. M., Kaul, S., and Skalak, T., C., 1998, " Delivery of colloidal Particles and red blood cells to tissue, through microvessel ruptures created by targeted micro bubble destruction with ultrasound " , Vol. 98 , pp. 1264-1267.
7. Zearcic, Z., and Brenner, M. P., "Self-replicating colloidal clusters", PNAS, Vol.111 (5). pp. 1748-1753.
8. Iseraelachvili, J. N., 2011, "Intermolecular and surfaces forces", Academic Press.
9. Wensink, H. H., and Lowen, H., 2008, "Aggregation of self-propelled colloidal rods near confining walls", Physical Review E, Vol. 78(3), p. 031409.
10. Peruani, E., Deutsch, A., and Bar, M., 2008, "Non-equilibrium clustering of self-propelled rods", Physical Review E, Vol. 74(3), p.03094.
11. Martel, S., and Mohammadi, M., 2010, "Using a swarm of self-propelled natural microrobots in the form of flagellated bacteria to perform complex micro-assembly tasks", Robotics and Automation, IEEE International Conference, pp. 500-505.
12. Maggi, C., Simmchen, J., Saglimbeni, F., Katuri, J., Dipalo, M., De Angelis, F., Sanchez, S. and Di Leonardo, R., 2016," Self-Assembly of Micromachining Systems Powered by Janus Micromotors", *Small*, *12*(4), pp.446-451.
13. Snezhko, A. and Aranson, I.S., 2011, "Magnetic manipulation of self-assembled colloidal asters", Nature materials, 10(9), pp.698-703.

14. Zhang, J., Yan, J. and Granick, S., 2016, "Directed Self-Assembly Pathways of Active Colloidal Clusters", Angewandte Chemie International Edition, 55(17), pp.5166-5169.
15. Yan, J., Han, M., Zhang, J., Xu, C., Luijten, E. and Granick, S., 2016, " Reconfiguring active particles by electrostatic imbalance", Nature Materials.
16. Brady, J. F., and Bossis, G., 1988, "Stokesian dynamics", Ann. Rev. Fluid Mech., Vol. 20, pp. 111-157.
17. Ladd, A. J. C., and Verberg, R., 2001, "Lattice-Boltzmann simulations of particle-fluid suspensions", Journal of Statistical Physics, Vol. 104(5-6), pp. 1191-1251.
18. Chan,Y, C., Beris, A.H., and Advani, S. G., 1992, "Second-order boundary element method calculations of hydrodynamic interactions between particles in close proximity", Internatinal Journal for Numerical Methods in Fluids, Vol. 14, pp. 1063-1086.
19. Keaveny, E. E., and Maxey, M. R., 2008, "Spiral swimming of an artificial micro-swimmer", Journal of fluid Mechanics, Vol. 598, pp. 293-319.
20. Ishikawa, T., Simmonds, M., P., and Pedley, T. J., 2006, "Hydrodynamic interaction of two swimming model micro-organism", Journal of Fluid Mechanics, Vol. 568, pp. 119-160.
21. Swan, J.W. Bready, J. F., Moore, R. S., and CHE174, 2011, " Modeling hydrodynamic self-propulsion with Stokesian dynamics or teaching Stokesian dynamics to swim", Physics of Fluids, Vol. 23(7), p.071901.
22. Jeffrey, D.J. and Onishi, Y., 1984," Calculation of the resistance and mobility functions for two unequal rigid spheres in low-Reynolds-number flow", Journal of Fluid Mechanics, 139, pp.261-290.
23. Durlofsky, L., Brady, J. F., and G. Bossis, 1987, "Dynamic simulation of hydrodynamically interacting particles", Journal of Fluid Mechanics, Vol. 180, pp. 21-49.
24. Chwang, A. T., & Wu, T. 1975, "Hydromechanics of low-Reynolds-number flow. Part 2. Singularity method for Stokes flows", Journal of Fluid Mechanics, Vol. 67, pp. 787-815
25. Wozniak M., Onofri F., Barbosa S., Yon J., Mroczka J., 2012," Comparison of methods to derive morphological parameters of multifractal samples of particle aggregates from TEM images", Journal of Aerosol Science, vol. 47, pp. 12-26.
26. Dreaden, E. C., Kong, Y. W., Morton, S. W., Correa, S., Choi, K. Y., Shopsowitz, K. E., ... & Hammond, P. T. (2015),"Tumor-Targeted Synergistic Blockade of MAPK and PI3K from a Layer-by-Layer Nanoparticle", Clinical Cancer Research, Vol.21(19), 4410-4419.

N	$\overline{U}_{Kf=2.1}$	$\overline{U}_{Kf=2.4}$	$\frac{(\overline{U})_{Kf=2.1}}{(\overline{U})_{Kf=2.4}}$
100	0.009071	0.004946	1.833997
150	0.011113	0.00419	2.652423
200	0.004955	0.003842	1.28949
250	0.008301	0.001485	5.591003
300	0.002046	0.001895	1.079756
350	0.002131	0.003457	0.616478
400	0.003915	0.00335	1.168803

Table 1 The swimming velocity of the cluster for the case of different fractal dimensions with U_s applied in the x-direction.

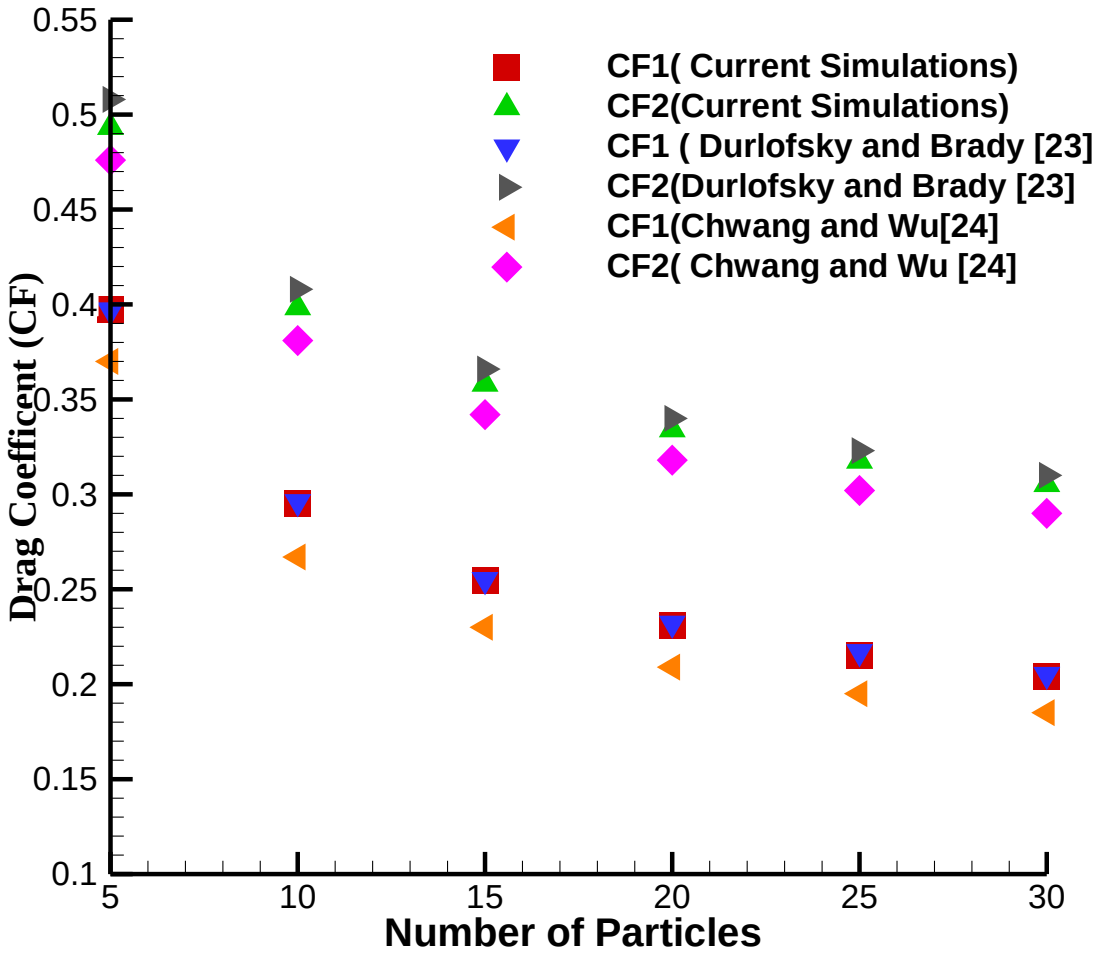

Figure 1 Comparison of the drag coefficient obtained from the current computer code and those from the literature.

(a) N = 100

(b) N = 200

(c) N = 300

(d) N = 400

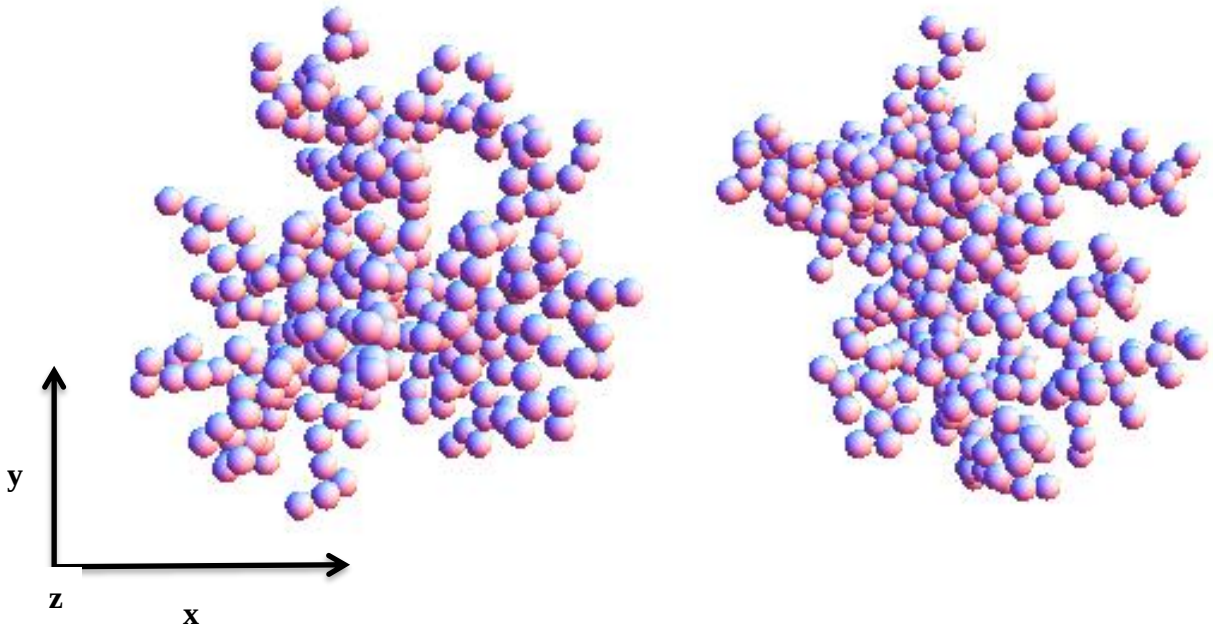

Figure 2 The initial configuration of the clusters for different number of particles and Kf = 2.1.

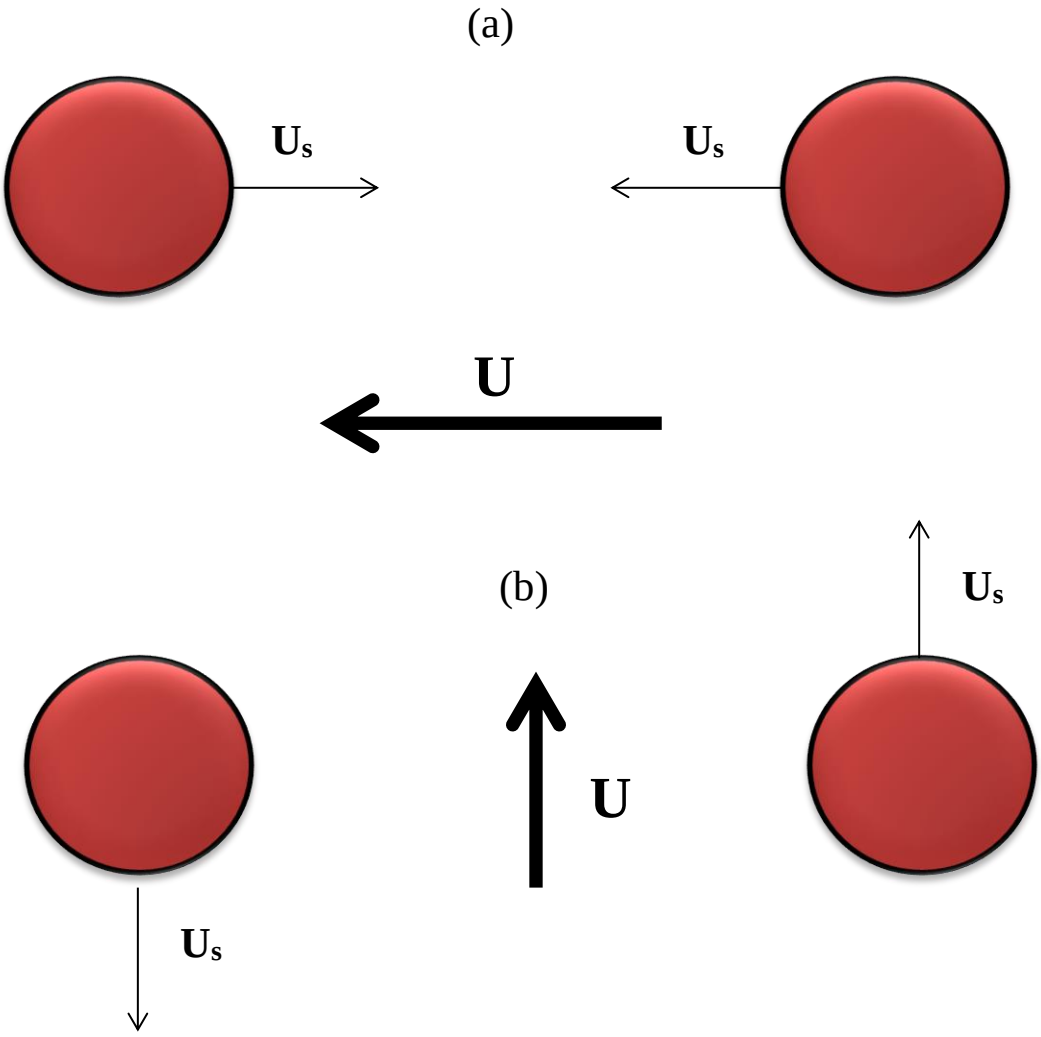

Figure 3 Explicit gait velocity U_s(a)in the x direction, (b) in the y direction, and the resulted swimming velocity.

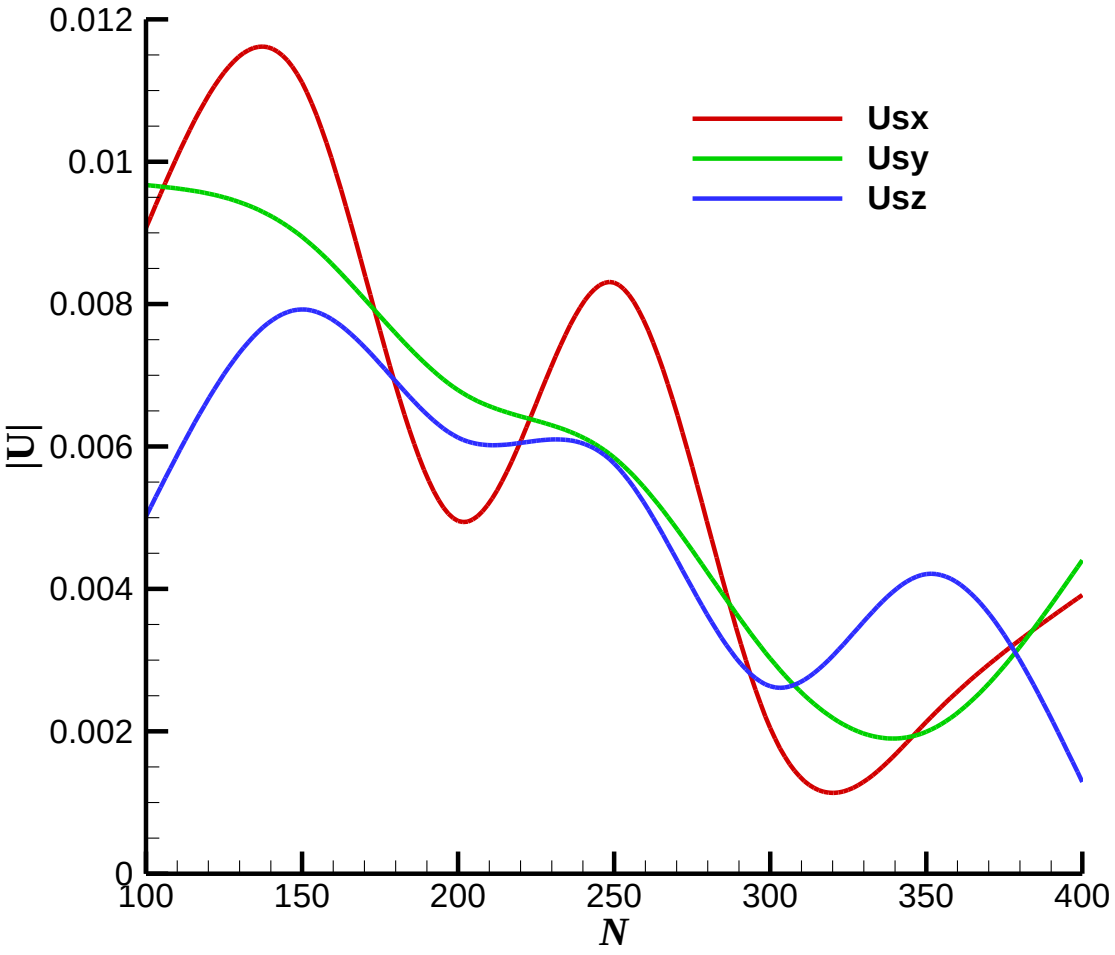

Figure 4 Variation of the swimming velocity with respect to the number of particles for different explicit gait velocity orientation and Kf = 2.1.

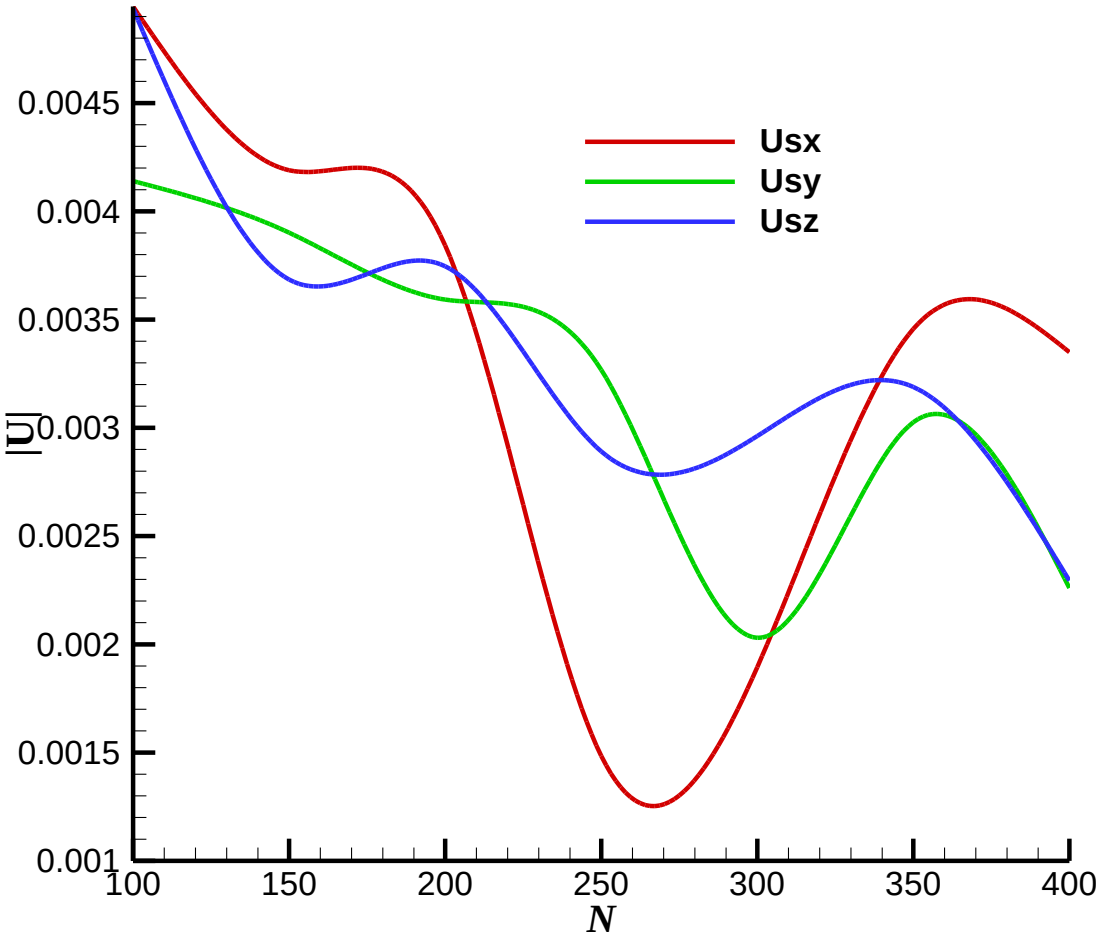

Figure 5 Variation of swimming velocity with respect to the number of particles for different explicit gait velocity orientation and Kf = 2.4.

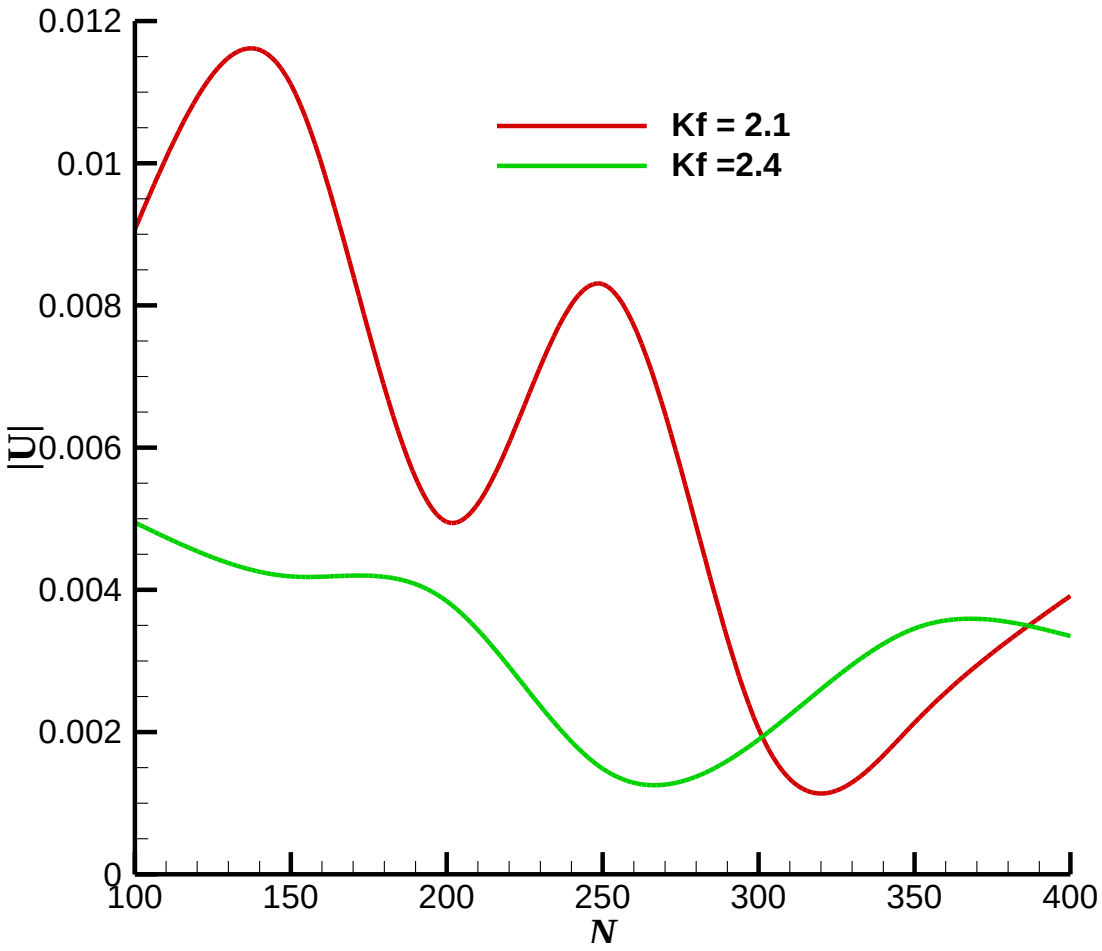

Figure 6 Comparison between the swimming velocity of DLA clusters for different fractal dimensions (Kf =2.1, 2.4), explicit gait velocity applied in the x – direction.

(a) N= 100, Kf = 2.1

(b) N = 100, Kf = 2.4

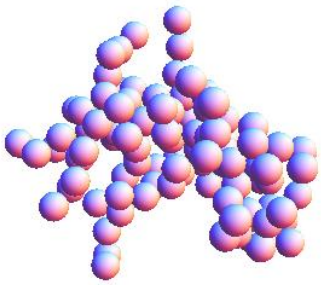

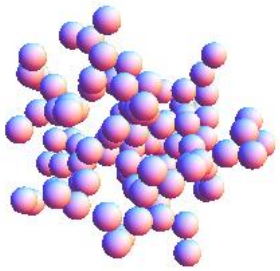

(c) N = 250, Kf = 2.1

(d) N= 250, Kf = 2.4

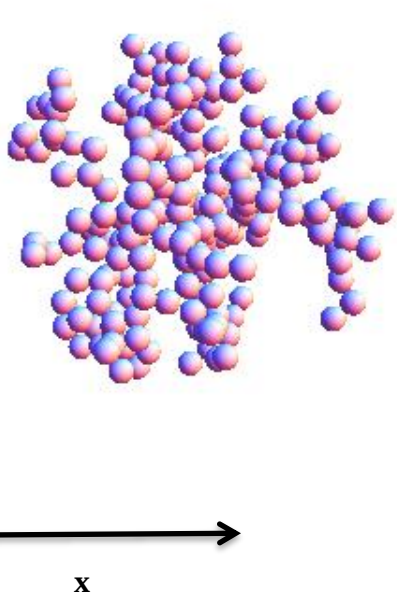

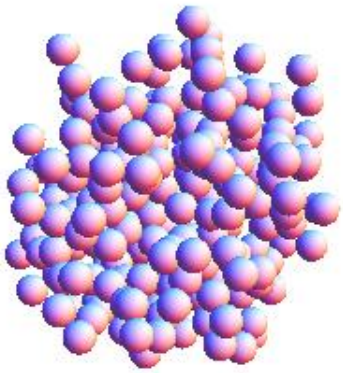

Figure 7 Comparison between the initial configuration of the clusters for fractal dimensions of 2.1 and 2.4.

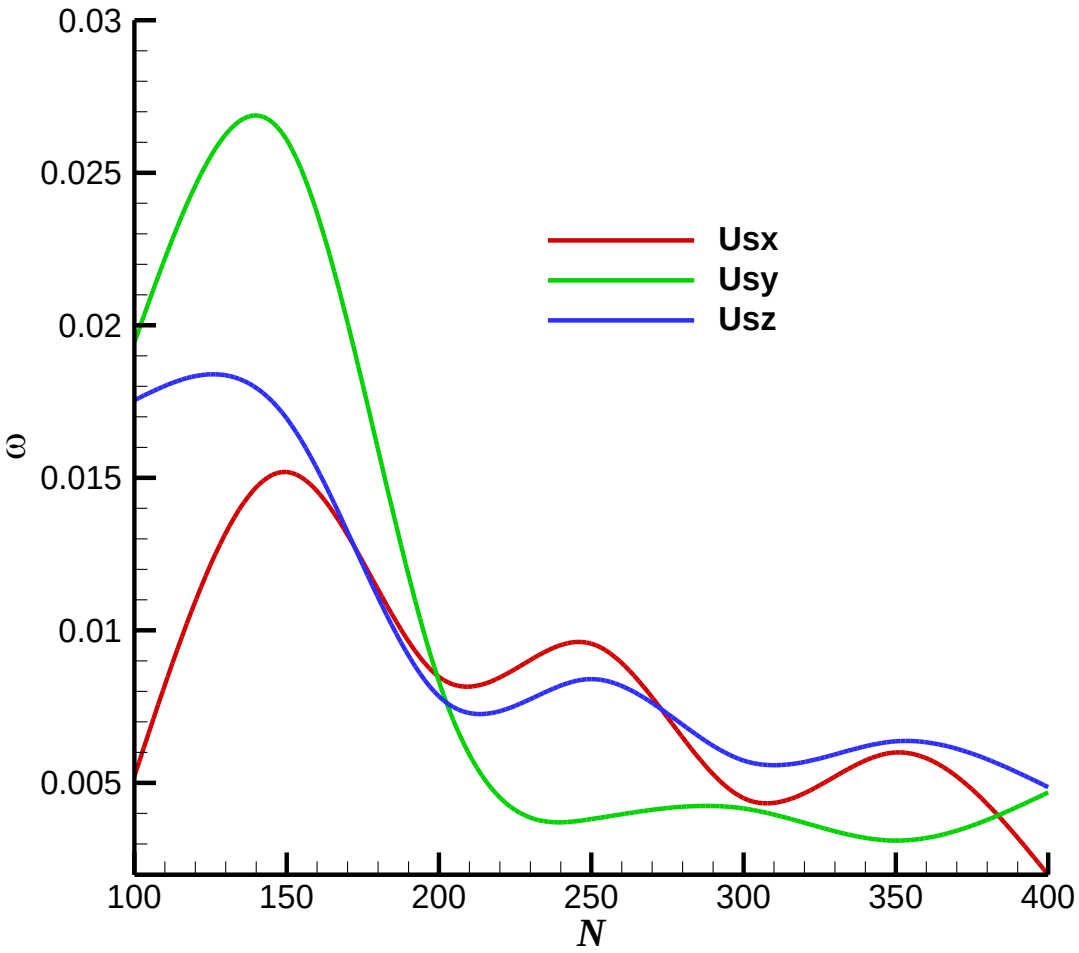

Figure 8 Variation of the angular swimming velocity with respect to the number of particles for different explicit gait velocity orientation and Kf = 2.1.

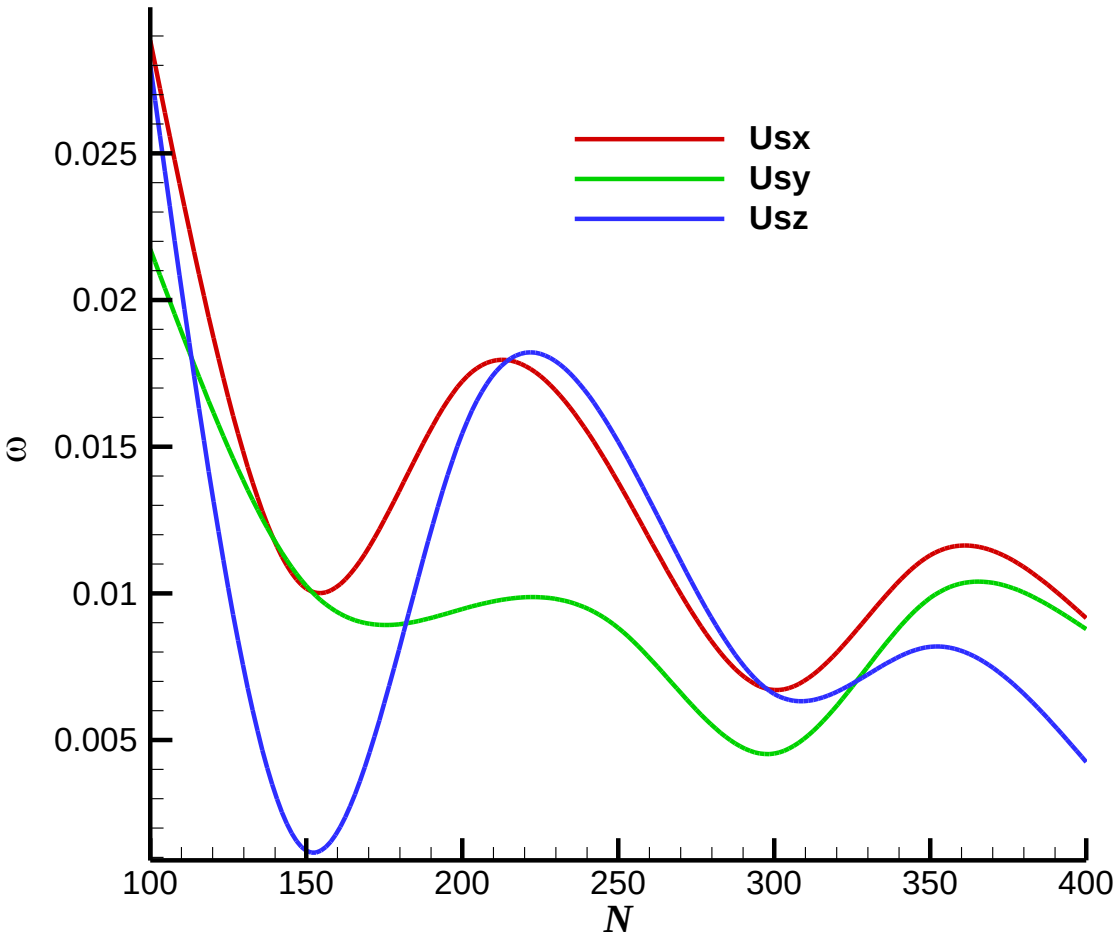

Figure 9 Variation of the angular swimming velocity with respect to the number of particles for different explicit gait velocity orientation and Kf = 2.4.

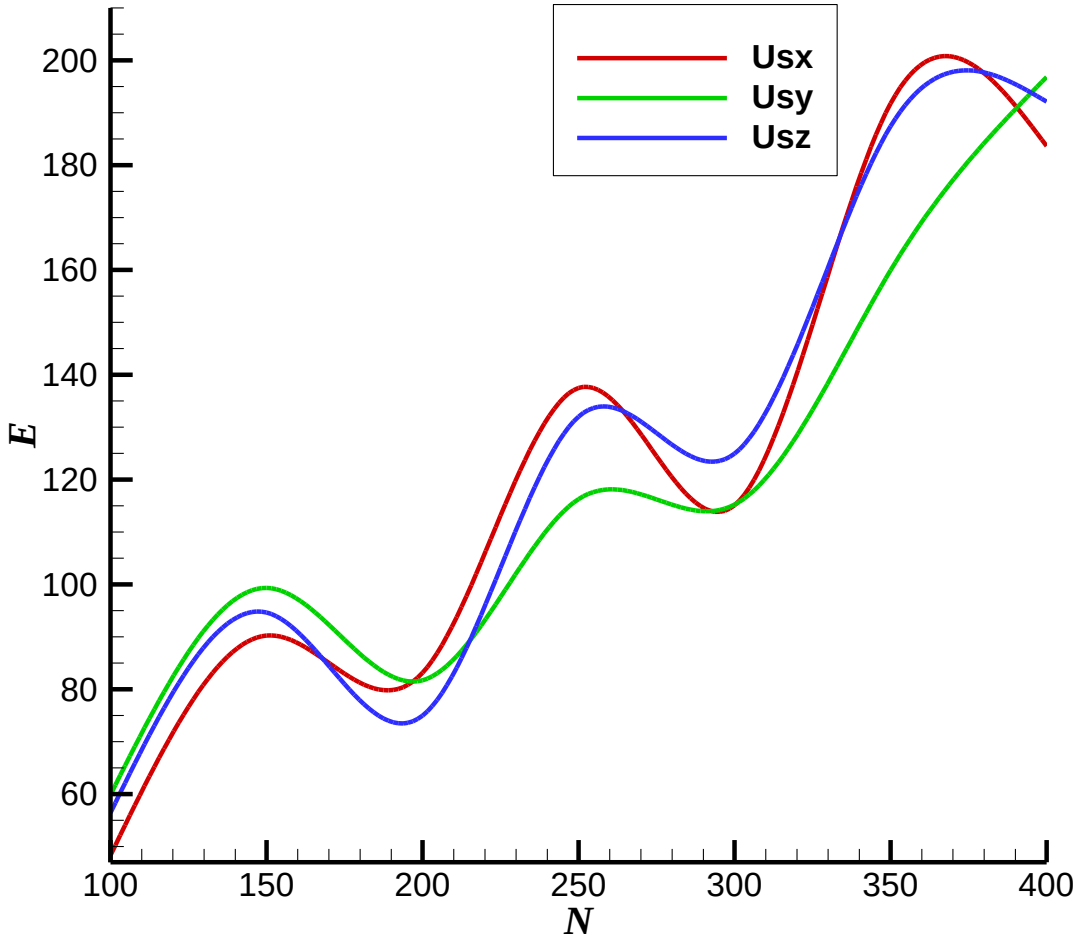

Figure 10 Variation of non-dimensional energy dissipation rate with respect to the number of particles for different explicit gait velocity orientation and Kf = 2.1.

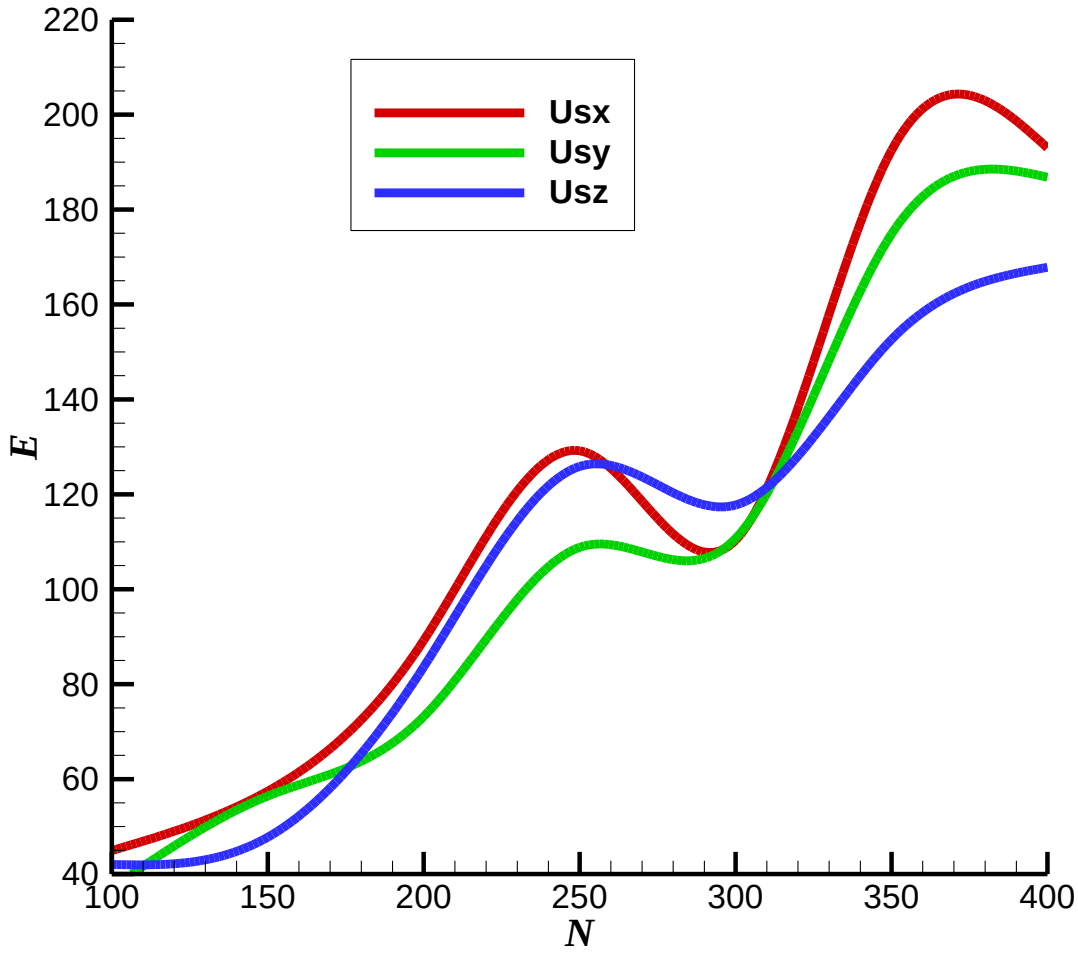

Figure 11 Variation of non-dimensional energy dissipation rate with respect to the number of particles for different explicit gait velocity orientation and Kf = 2.4.

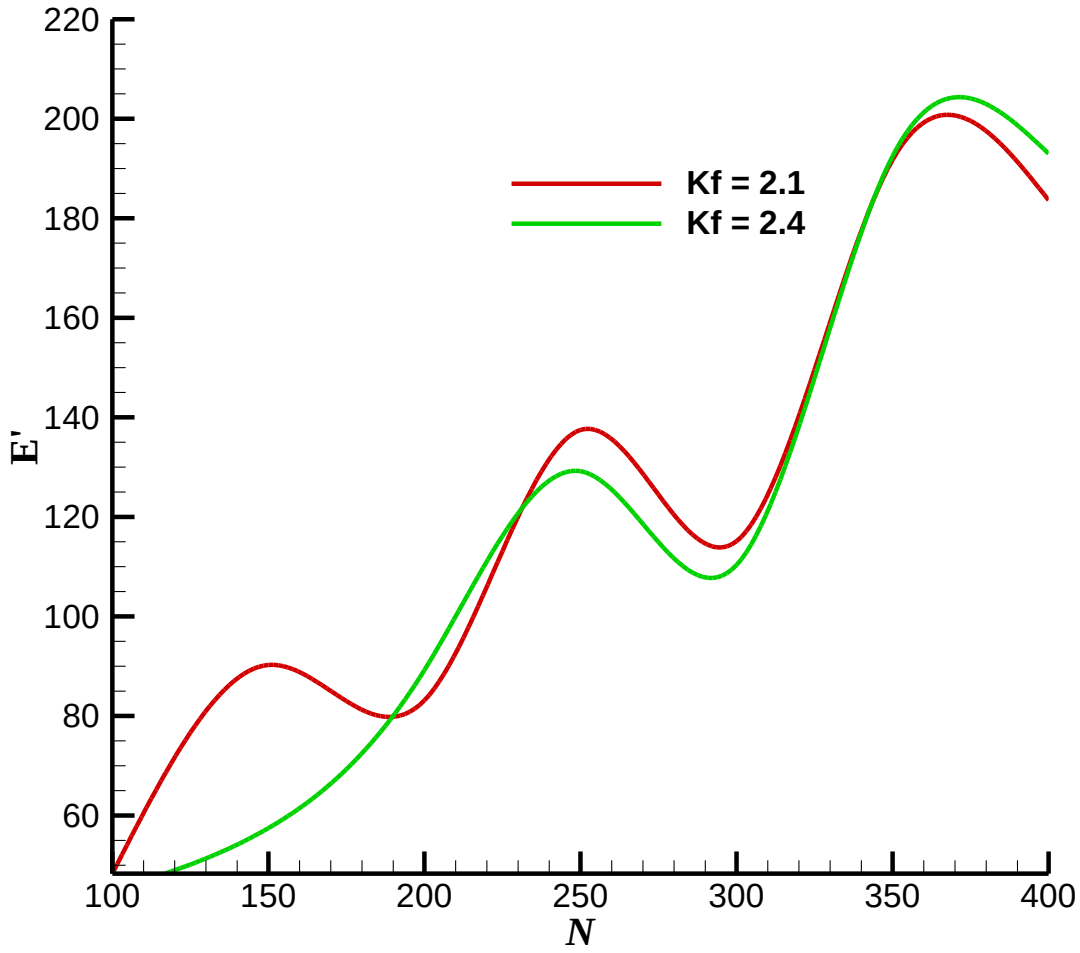

Figure 12 Comparison between the non-dimensional energy dissipation of DLA clusters for different fractal dimensions (Kf= 2.1, 2.4), explicit gait velocity applied in the x – direction.

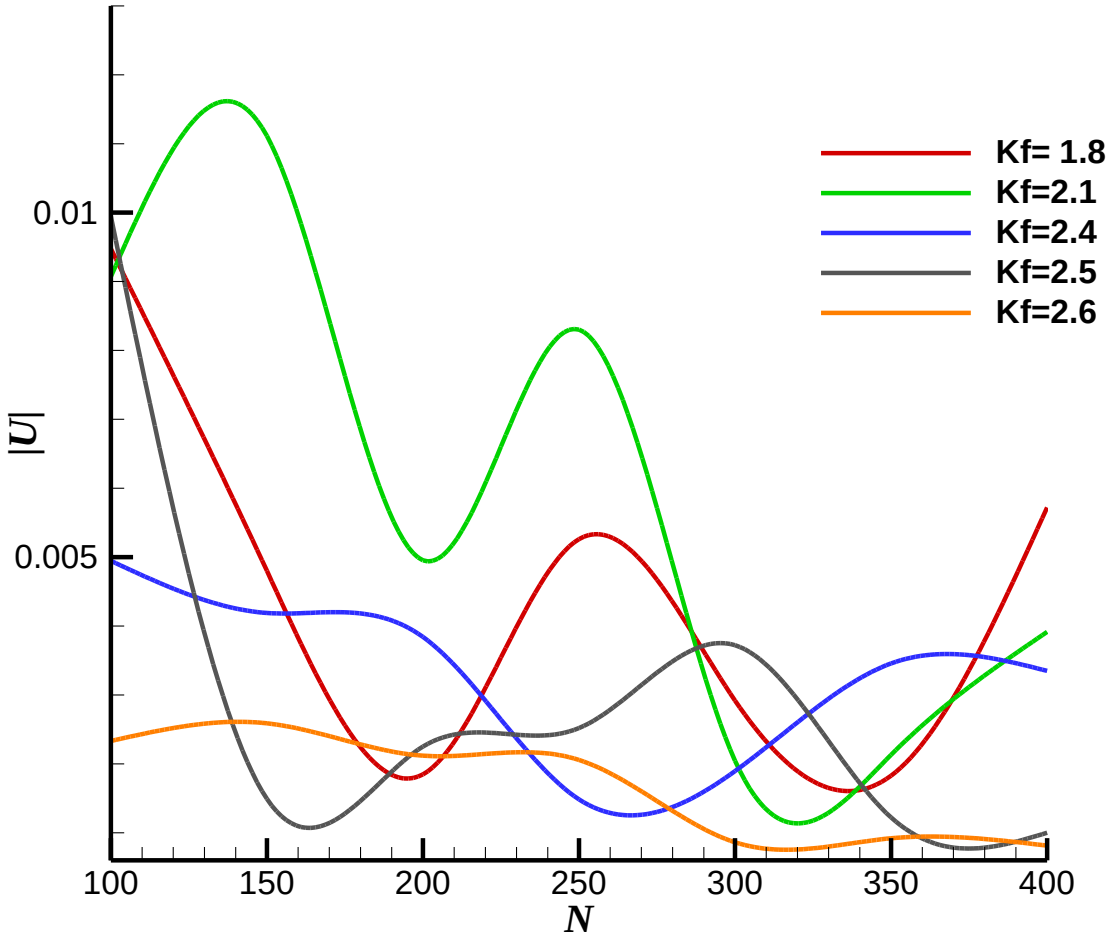

Figure 13 Comparison between the swimming velocity of DLA clusters for different fractal dimensions explicit gait velocity applied in the x direction.

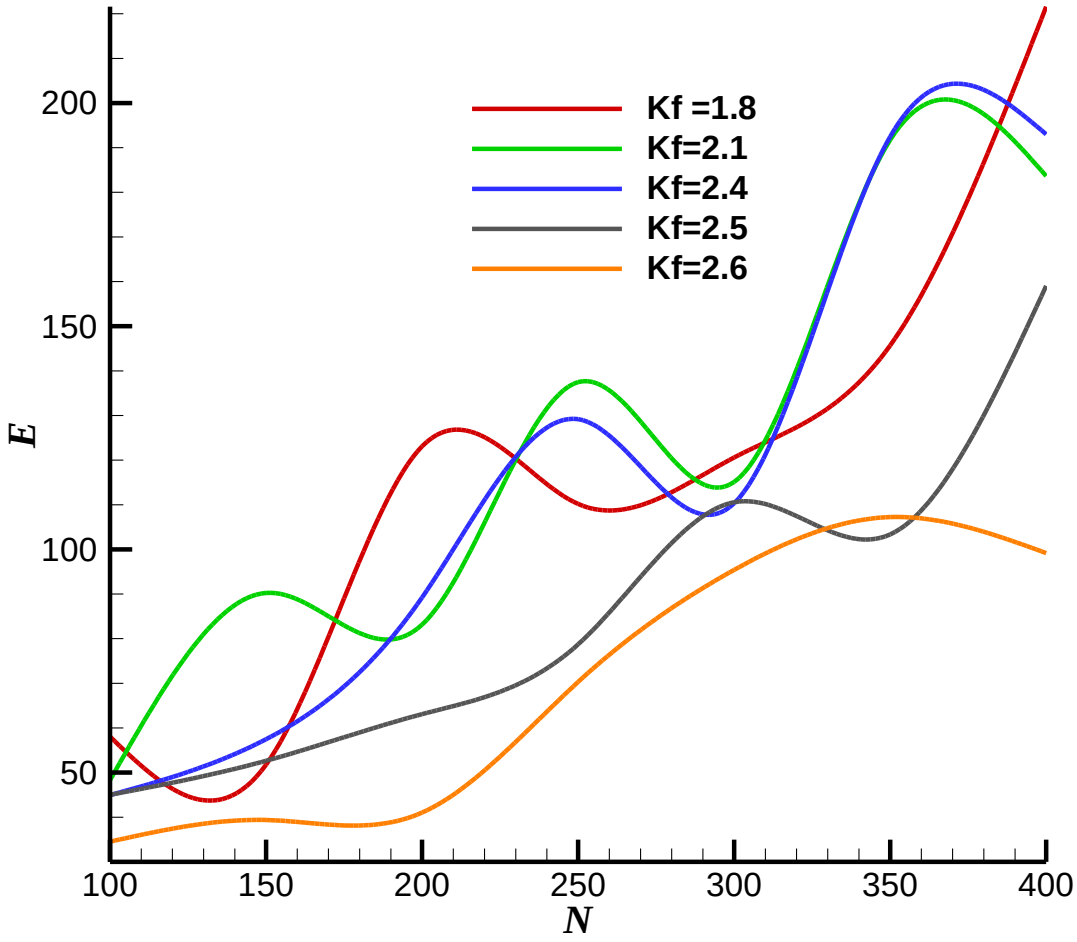

Figure 14 Comparison between the non-dimensional energy dissipation of DLA clusters for different fractal dimensions explicit gait velocity applied in the x direction